

Twisted coupled wire model for a moiré sliding Luttinger liquid

Yichen Hu¹, Yuanfeng Xu^{1,2}, and Biao Lian¹

¹Department of Physics, Princeton University, Princeton, New Jersey 08544, USA

²Center for Correlated Matter and School of Physics, Zhejiang University, Hangzhou, 310058, China

Recent experiments in twisted bilayer WTe_2 revealed the existence of anisotropic Luttinger liquid behavior. To generically characterize such anisotropic twisted bilayer systems, we study a model of a twisted bilayer of two-dimensional (2D) arrays of coupled wires, which effectively form an array of coupled moiré wires. We solve the model by the transfer matrix method, and identify quasi-1D electron bands in the system at small twist angles. With electron interactions added, we show that the moiré wires have an effective Luttinger parameter g_{eff} lower than that of the microscopic wires. This leads to a sliding Luttinger liquid (SLL) temperature regime, in which power-law current voltage relations arise. For parameters partly estimated from WTe_2 , a microscopic interaction $U \sim 3\text{eV}$ yields a temperature regime of SLL similar to that in the WTe_2 experiments.

One-dimensional (1D) interacting electrons form Luttinger liquids[1–6], which show non-Fermi liquid physics such as spin-charge separation and power-law voltage-current relations violating the Ohm's law. In highly anisotropic 2D electron systems, it was proposed that interactions can lead to a sliding Luttinger liquid (SLL) phase or regime [7–25], which shows quasi-1D physics analogous to the 1D Luttinger liquid[26–29]. Recent studies of moiré systems of twisted homobilayer or heterobilayer 2D materials have enabled engineering of a rich variety of 2D electron systems, such as flat bands with strong interactions [5, 29–46]. Intriguingly, in the twisted bilayer WTe_2 which hosts a rectangular moiré pattern, transport experiments [28, 29] reveal a phase that exhibits (1) a strong in-plane electronic anisotropy, (2) a power-law scaled conductance in the hard direction and (3) a nonlinear differential resistance that vanishes at zero bias in the easy direction. The phenomena strongly suggests quasi-1D physics in a SLL regime. The tunability of moiré systems may allow a thorough exploration of the physics of SLLs. Therefore, it is important to understand theoretically the mechanism of quasi-1D SLLs from twisted bilayer anisotropic systems, and to investigate its dependence on twist angles and interaction strengths.

In this paper, we study a model of a twisted bilayer of 2D arrays of coupled wires, which effectively forms a network model with interwire and interlayer hoppings. The goal of the model is to give a simplified generic description of twisted bilayer anisotropic systems, and investigate the emergence of an array of coupled moiré wires showing SLL physics. At small twist angles, the model can be solved from the real space transfer matrix, which directly gives the Fermi surface of moiré bands at the Fermi energy. We find that compared to the microscopic coupled wires, the emergent coupled moiré wires show much smaller Luttinger parameter g_{eff} , implying much stronger correlation effects. For parameters partly estimated from WTe_2 , a microscopic interaction $U \gtrsim 3\text{eV}$ yields an SLL temperature regime around that in experiments.

The single-particle model. Monolayer WTe_2 has an anisotropic crystal structure and an anisotropic band structure, as shown in Fig. 1(a). In the valence band which is relevant to SLL experimentally [28, 29], the W atom orbitals dominate. In real space, the W atoms approximately form arrays of quasi-1D wires [along the horizontal direction in Fig. 1(b)]. In twisted bilayer WTe_2 , the W atom quasi-1D wires of the

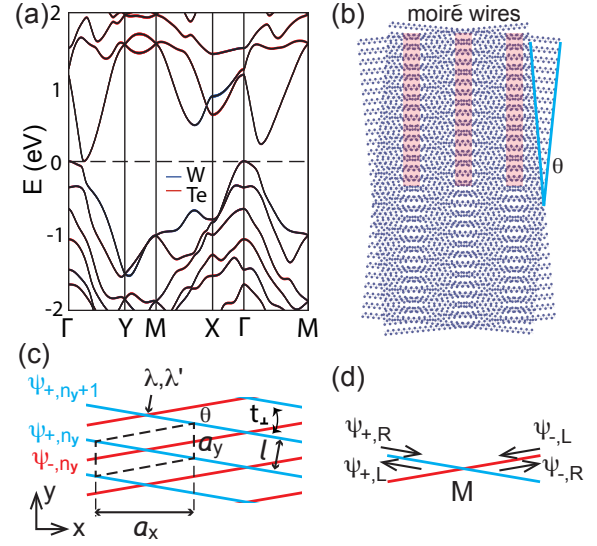


FIG. 1. (a) DFT band structure of monolayer WTe_2 , showing domination by W orbitals in the valence band around the Γ point. (b) W atom positions in twisted bilayer WTe_2 , and illustration of the emergent moiré wires. (c) Twisted network model consisting of two arrays of coupled wires with a twist angle θ . Dotted lines encircle a moiré unit cell. (d) Zoom-in around a single interlayer intersection point, across which the wavefunctions are related by transfer matrix M .

two layers form a moiré pattern in Fig. 1(b), which visually show effective vertical moiré wires at a larger length scale.

To give a generic simplified single-particle model of an anisotropic moiré system such as twisted bilayer WTe_2 , we approximate each layer by an array of coupled wires with interwire distance l as shown in Fig. 1(c), where the blue and red wires are in the upper and lower layers, respectively. The two layers differ by a twist angle θ . We assume the electrons (or holes via a particle-hole transformation) in each wire have a quadratic dispersion with an effective mass m , and a hopping $-t_{\perp}$ between two nearest neighbor wires in each layer. Since the relevant hole band in WTe_2 is around the Γ point, the spin-orbital coupling can be neglected (as is known for transition-metal dichalcogenides [47, 48]), and thus we can

choose t_\perp to be real. As shown in Fig. 1(c), the wires of the two layers cross at positions with x coordinates $x = n_x a_x$, where $n_x \in \mathbb{Z}$, and $a_x = \frac{l}{2 \sin(\theta/2)}$. The vertical distance between two neighboring wires in each layer is $a_y = \frac{l}{\cos(\theta/2)}$. At each crossing of two wires from two layers [Fig. 1(d)], we assume a delta function intralayer potential of strength λ and a delta function interlayer hopping of strength λ' . For small twist angle θ , we can approximate the coordinate along each wire by x , and we use $\psi_{\alpha, n_y}(x)$ to denote the wavefunction in the n_y -th wire ($n_y \in \mathbb{Z}$) in layer $\alpha = \pm$. Note that because of the relative twisting, the n_y -th wire in layer α crosses with the $(n_y - \alpha n_x)$ -th wire in layer $-\alpha$ at $x = n_x a_x$. The single-particle Schrödinger equation at energy E (measured from band bottom) is then

$$E\psi_{\alpha, n_y} = \left(2t_\perp - \frac{\hbar^2 \partial_x^2}{2m}\right) \psi_{\alpha, n_y} - t_\perp (\psi_{\alpha, n_y+1} + \psi_{\alpha, n_y-1}) + \delta(x - n_x a_x) (\lambda \psi_{\alpha, n_y} + \lambda' \psi_{-\alpha, n_y - \alpha n_x}). \quad (1)$$

While this oversimplified model does not correspond to a concrete material, our goal is to understand how moiré patterns generically give rise to SLL physics. Hereafter, to reflect the physics of twisted bilayer WTe_2 as much as possible, we take $l = 0.627\text{nm}$, interlayer distance $a_z = 0.77\text{nm}$, and $m = 0.38m_e$ where m_e is the bare electron mass, as estimated for the W atom chains in WTe_2 from density functional theory (DFT). For the effective interwire hoppings, we take $t_\perp = 20\text{meV}$, $\lambda = 10\text{meV} \cdot \text{nm}$ and $\lambda' = 20\text{meV} \cdot \text{nm}$, based on the order of magnitude of direct hopping between W atoms in DFT [see Appendix C and D for details (see also references[49–51] therein)]. However, we do not expect the above effective parameters to characterize WTe_2 quantitatively, which experimentally shows substantial deviations from DFT in some aspects, possibly due to strong interactions[52–59]

The Schrödinger Eq. (1) for small θ can be most easily solved by the transfer matrix method. We consider the transfer matrix in the x direction for a state with energy E and quasimomentum q_y in the y direction. For $(n_x - 1)a_x < x < n_x a_x$, such a state takes the form

$$\begin{aligned} \psi_{\alpha, n_y}(x) &= e^{iq_y a_y (n_y - \frac{\alpha}{2} n_x)} \tilde{\psi}_{\alpha, q_y}^{n_x}(x), \\ \tilde{\psi}_{\alpha, q_y}^{n_x}(x) &= e^{ik(x - n_x a_x)} \varphi_{\alpha, q_y}^{n_x, R} + e^{-ik(x - n_x a_x)} \varphi_{\alpha, q_y}^{n_x, L}, \end{aligned} \quad (2)$$

where $k = \hbar^{-1} \sqrt{2m[E + 2t_\perp(\cos(q_y a_y) - 1)]}$ is the free momentum along the wire, and $\varphi_{\alpha, q_y}^{n_x, R}$ and $\varphi_{\alpha, q_y}^{n_x, L}$ are the right-moving and left-moving amplitudes, respectively. By re-organizing the wavefunction into a four-component vector $\Psi_{q_y, n_x} = (\varphi_{+, q_y}^{n_x, L}, \varphi_{+, q_y}^{n_x, R}, \varphi_{-, q_y}^{n_x, L}, \varphi_{-, q_y}^{n_x, R})^T$, the Schrödinger equation can be reformulated into the transfer matrix equation (Appendix A)

$$\Psi_{q_y, n_x+1} = T(E, q_y) \Psi_{q_y, n_x}. \quad (3)$$

The transfer matrix can be further decomposed into two parts, $T(E, q_y) = Q(E, q_y)M(E, q_y)$, where $Q(E, q_y) =$

$\text{diag}(e^{-ika_x}, e^{ika_x}, e^{-ika_x}, e^{ika_x})$ is the diagonal propagation matrix, and one can show that

$$M(E, q_y) = \begin{pmatrix} (\sigma_0 - \frac{i\lambda' m}{k} s_0) e^{i\frac{q_y}{2}} & -\frac{i\lambda m}{k} s_0 e^{i\frac{q_y}{2}} \\ -\frac{i\lambda m}{k} s_0 e^{-i\frac{q_y}{2}} & (\sigma_0 - \frac{i\lambda' m}{k} s_0) e^{-i\frac{q_y}{2}} \end{pmatrix} \quad (4)$$

is the scattering matrix at the node, where σ_0 is the 2×2 identity matrix, and $s_0 = \sigma_z + i\sigma_y$ in terms of the 2×2 Pauli matrices $\sigma_{x,y,z}$.

One can solve the eigenvectors of the transfer matrix $T(E, q_y)$, and we denote the eigenvalue as $e^{iq_x a_x}$:

$$T(E, q_y) \tilde{\Psi}_{q_y, q_x} = e^{iq_x a_x} \tilde{\Psi}_{q_y, q_x}. \quad (5)$$

If q_x is real, the eigenvector $\tilde{\Psi}_{q_y, q_x}$ gives an eigenstate of the Schrödinger Eq. (1), with quasimomentum q_x in the x direction and q_y in the y direction.

Taking $E = E_F$ to be the Fermi energy, the above procedure naturally gives the Fermi surface of the band structure in the quasimomentum (q_x, q_y) space. The transfer matrix is thus advantageous if one focuses on the low energy states near the Fermi surface. Fig. 2(a) shows the Fermi surface (black lines) calculated for $E_F = 30\text{meV}$ at 5° (left) and 3° (right). Fig. 2(b) shows zoomed in image of bands boxed in red dotted lines in 3° Fermi surface. As shown in Fig. 2(a), there are Fermi surfaces forming a periodic loop in the q_x direction, indicating that these bands are highly quasi-1D, with effective coupled moiré wires as shown in Fig. 1(b). We focus on the band with the flattest Fermi surface. We characterize the anisotropy of the band by the dimensionless number $a_y \Delta q_y / \pi$, where Δq_y is the width of q_y spanned by the Fermi surface dispersion shown in Fig. 2(b). This anisotropy as a function of twist angle θ for different E_F is shown by the black lines in Fig. 2(c). We note that such quasi-1D Fermi surfaces forming loops in q_x only occur below a certain twist angle θ_c , for instance, $\theta_c \approx 6.3^\circ$ for $E_F = 30\text{meV}$. Moreover, we can numerically calculate the Fermi velocity of the band $v_F = dE/dq_y$ at $q_x = 0$ by slightly varying E and q_y . The Fermi velocity v_F as a function of θ for different E_F is given in Fig. 2(d).

We can estimate the effective y direction hopping energy of a moiré wire in Fig. 1(b) by $\tilde{t}_\perp = \pi v_F / a_y$, using the fact that π/a_y is the half Brillouin zone size in the y direction. The effective hopping across two nearest moiré wires can be estimated by $\tilde{t}_\perp = v_F \Delta q_y$, which is the energy scale inducing the Fermi surface dispersion of width Δq_y . Therefore, the anisotropy of effective coupled moiré wires in Fig. 2(c) is also equal to

$$\tilde{t}_\perp / \tilde{t}_\parallel = a_y \Delta q_y / \pi. \quad (6)$$

The smaller $\tilde{t}_\perp / \tilde{t}_\parallel$ is, the more quasi-1D in y direction the moiré band is.

Interaction effect. We now add electron-electron interaction to the model, and examine the emerging SLL physics in the moiré scale. The emergent quasi-1D moiré bands in the above model provide fertile ground for interaction induced correlations. In the microscopic lattice scale, we consider a

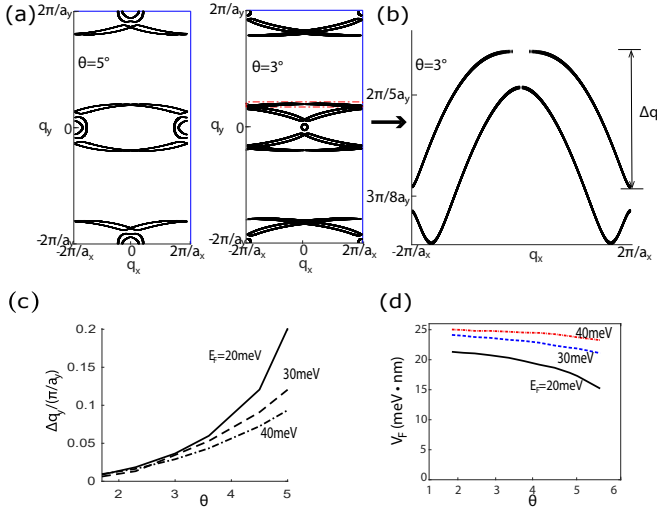


FIG. 2. (a) Fermi surface solved for $\theta = 5^\circ$ (left) and $\theta = 3^\circ$ (right) twisted model with Fermi energy $E_F = 30\text{meV}$, using transfer matrix method (with parameters given below Eq. (1)). (b) Zoomed-in plot of red dotted region of the 3° Fermi surface in (a). Δq_y characterizes the flatness of q_x -direction dispersion of the band. (c) $\frac{\Delta q_y}{\pi/a_y}$ versus θ for different E_F . (d) Fermi velocity v_F versus angle θ for different Fermi energy E_F .

generic *spin-independent* anisotropic screened repulsive interaction between two electrons with distance \mathbf{r} (both intralayer and interlayer):

$$V_I(\mathbf{r}) = U \exp\left(-\sqrt{\frac{x^2}{x_0^2} + \frac{y^2}{y_0^2} + \frac{z^2}{z_0^2}}\right). \quad (7)$$

In a 2D Thomas-Fermi screening model of Coulomb interaction, the screening length is estimated as $r_0 = \frac{2\pi\epsilon_r\epsilon_0\hbar^2}{e^2m}$ along a direction with effective mass m , where e is the electric charge. Along the x -direction, taking $\epsilon_r \approx 10$ (which is approximately the value for WTe_2 [60]), and effective mass $m = 0.38m_e$, one arrives at a screening length $x_0 \sim 1\text{nm}$. The quasi-1D nature (along the x direction) of the microscopic system gives heavier effective masses (by approximately one order of magnitude) along the y and z directions, so we take $y_0 = 5\text{nm}$, $z_0 = 10\text{nm}$. We note that for low carrier densities with which we are concerned, the bare interaction energy scale is likely larger than the electron kinetic energy, so the Thomas-Fermi model may overestimate the screening. Nevertheless, as a model study, we fix x_0 , y_0 , and z_0 as above, and leave the microscopic interaction U as a tuning parameter. For reference, taking $V_I(x_0, 0, 0) \sim \frac{e^2}{4\pi\epsilon_0 x_0}$ yields a U of order 5eV .

For a 1D moiré wire, the electrons with interaction becomes a Luttinger liquid with spin-charge separation. The charge Luttinger parameter g_{eff} and spin Luttinger parameter $g_{\text{eff},s}$ are

given by [4, 61]

$$g_{\text{eff}} = \sqrt{\frac{2\pi v_F + \tilde{V}(2q_F)}{2\pi v_F + 2\tilde{V}(0) - \tilde{V}(2q_F)}}, \quad (8)$$

$$g_{\text{eff},s} = \sqrt{\frac{2\pi v_F + \tilde{V}(2q_F)}{2\pi v_F - \tilde{V}(2q_F)}},$$

where $\tilde{V}(0)$ and $\tilde{V}(2q_F)$ are the interaction strength in the quasimomentum q_y space for scattering with zero momentum change (forward scattering) and $2q_F$ momentum change (back scattering), respectively (see Appendix B), and $v_F = dE/dq_y$ is the Fermi velocity. For repulsive interaction, one usually has $\tilde{V}(0) > \tilde{V}(2q_F)$ and $\tilde{V}(0) > 0$, thus $g_{\text{eff}} < 1$. For the parameters we choose, we find $|\tilde{V}(2q_F)| \sim 10^{-3}\tilde{V}(0) \ll v_F$, so the spin Luttinger parameter is always approximately $g_{\text{eff},s} \approx 1$.

We average over pairs of Fermi surface states at quasimomenta $(q_x, \pm q_F(q_x))$ to obtain the average charge Luttinger parameter g_{eff} . Fig. 3(a) shows g_{eff} as a function of E_F calculated for $U = 3\text{eV}$ and twist angle $\theta = 5^\circ$, which is below 0.3. The effective hopping t_\perp between neighboring moiré wires is also plotted. Fig. 3(b) shows how g_{eff} depends on the interaction strength U as a function of θ , where $E_F = 30\text{meV}$. We find that g_{eff} increases as θ decreases. This is because the width a_x of a moiré wire increases as θ decreases, and thus two electrons in the moiré wire have less chance to scatter with each other, leading to a weaker effective interaction. In comparison, for a microscopic decoupled wire in a monolayer, which has a Fermi momentum $k_F = \sqrt{2mE_F}$, we can estimate its microscopic Luttinger parameter g similarly to Eq. (8), which is generically larger ($g \gtrsim 0.6$) than the moiré effective Luttinger parameter g_{eff} here given the same U .

The moiré SLL regime. The temperature regime for SLL physics depends on the effective moiré parameters t_\perp , t_\parallel , and g_{eff} [10, 11, 25, 62], which we explain below. Without the interwire hopping t_\perp , and setting $g_{\text{eff},s} = 1$, each moiré wire along the y direction has a zero-temperature 1D Luttinger liquid Green's function following[63]

$$G_\zeta^{1D}(y, t) = \langle \mathcal{T} \hat{\psi}_{n_x, \zeta}(y, t) \hat{\psi}_{n_x, \zeta}^\dagger(0, 0) \rangle$$

$$= \frac{1}{2\pi} (y - \zeta v_c t + i\zeta 0^+)^{-\frac{1}{2}} (y - \zeta v_s t + i\zeta 0^+)^{-\frac{1}{2}} \quad (9)$$

$$\times (y^2 - v_c^2(t - i0^+)^2)^{-\frac{\eta}{2}},$$

where $\zeta = \pm$ stands for the modes moving in the $\pm y$ directions, respectively, the charge mode has velocity $v_c = \frac{1}{2\pi} \sqrt{[2\pi v_F + \tilde{V}(0)]^2 - [\tilde{V}(2q_F) - \tilde{V}(0)]^2}$, the spin mode has velocity $v_s = \frac{1}{2\pi} \sqrt{4\pi^2 v_F^2 - \tilde{V}(2q_F)^2} \approx v_F$,

and the anomalous exponent $\eta = (g_{\text{eff}} + g_{\text{eff}}^{-1} - 2)/4$. In particular, $\eta = 0$ in the non-interacting $g_{\text{eff}} = 1$ limit. At low energies, the local density of states (spectral weight) scales as

$$\rho(\omega) = -\frac{1}{\pi} \text{Im} \sum_{\zeta=\pm} \tilde{G}_\zeta^{1D}(0, \omega) \propto \omega^\eta, \quad (10)$$

where $\tilde{G}_\zeta^{1D}(y, \omega)$ is the Fourier transform of Eq. (9) in time t . As can be seen by a simple power counting, the full Fourier transform of Eq. (9) in both y and t scales as $G_\zeta^{1D}(q, \omega) = \omega^{\eta-1} \tilde{t}_\perp^{-\eta} f(q/\omega)$ (which has the unit of inverse of energy), where $f(x)$ is some dimensionless function of order unity.

With the effective interwire hopping \tilde{t}_\perp , the hopping among different moiré wires can be incorporated as a self energy correction to Eq. (9). The zero-temperature Green's function is perturbatively given by a Schwinger-Dyson equation [62]:

$$G_\zeta(q, \omega) \approx G_\zeta^{1D}(q, \omega) + \tilde{t}_\perp G_\zeta^{1D}(q, \omega) G_\zeta(q, \omega) \approx \frac{G_\zeta^{1D}(q, \omega)}{1 - \tilde{t}_\perp G_\zeta^{1D}(q, \omega)}. \quad (11)$$

In the case $0 \leq \eta < 1$, for which the interaction is not too strong, $G_\zeta^{1D}(q, \omega) \propto \omega^{\eta-1} \tilde{t}_\perp^{-\eta}$ diverges in the low energy limit $\omega \rightarrow 0$. Clearly, the perturbation estimation Eq. (11) will break down when $\tilde{t}_\perp G_\zeta^{1D}(q, \omega) \sim \tilde{t}_\perp \tilde{t}_\parallel^{-\eta} \omega^{\eta-1} > 1$, namely, when the energy scale $\omega < \tilde{t}_\perp (\tilde{t}_\perp / \tilde{t}_\parallel)^{\frac{\eta}{1-\eta}}$. In this case, \tilde{t}_\perp can no longer be treated as a perturbation, and the system will behave as an intrinsically 2D system. For energy scales $\omega > \tilde{t}_\perp (\tilde{t}_\perp / \tilde{t}_\parallel)^{\frac{\eta}{1-\eta}}$, the Green's function in Eq. (11) resembles that of the 1D Luttinger liquid closely, and SLL quasi-1D behaviors are expected. In the case $\eta \geq 1$, $G_\zeta^{1D}(q, \omega)$ does not diverge as $\omega \rightarrow 0$, and thus the SLL quasi-1D behavior persists down to $\omega = 0$.

At finite temperature, the temperature T plays the role of the energy scale of the system, and thus the 1D Luttinger liquid Green's function $G_\zeta^{1D}(q, \omega) \propto (k_B T)^{\eta-1} \tilde{t}_\perp^{-\eta}$ in the low energy limit $\omega \rightarrow 0$, where k_B is the Boltzmann constant. Therefore, the quasi-1D SLL physics can only exist for temperatures $T > T_*$, where the lower bound crossover temperature for $0 \leq \eta < 1$ is

$$T_* \approx k_B^{-1} \tilde{t}_\perp (\tilde{t}_\perp / \tilde{t}_\parallel)^{\frac{\eta}{1-\eta}} \quad (12)$$

For $\eta \geq 1$, the SLL physics will persist down to $T_* = 0$.

In the SLL temperature regime $T > T_*$, the transverse conductivity σ_\perp across the moiré wires [namely, in the x direction in Fig. 1(c)] at temperature T is known to exhibit a power law scaling [7–12, 25]. Treating \tilde{t}_\perp as perturbation, σ_\perp is governed by the Kubo formula for tunneling between two neighboring wires:

$$\begin{aligned} \sigma_\perp(\omega, T) &\propto \tilde{t}_\perp^2 \int dy \int d\omega' \frac{n_f(\omega' + \omega) - n_f(\omega')}{\omega} \\ &\quad \times \text{Im} \tilde{G}_\alpha^{1D}(y, \omega') \text{Im} \tilde{G}_\alpha^{1D}(y, \omega + \omega') \\ &\propto \tilde{t}_\perp^2 T^{2\eta-1} F\left(\frac{\omega}{T}\right), \end{aligned} \quad (13)$$

where $F(x)$ approaches 1 as $x \rightarrow 0$, and scales as $x^{2\eta-1}$ as $x \gg 1$. For transverse transport measurement with voltage V between two neighboring moiré wires, the energy scale ω can be identified with V . Therefore, the transverse conductivity

$$\sigma_\perp(V, T) \propto \begin{cases} V^{2\eta-1}, & (eV > k_B T) \\ T^{2\eta-1}, & (eV < k_B T) \end{cases} \quad (14)$$

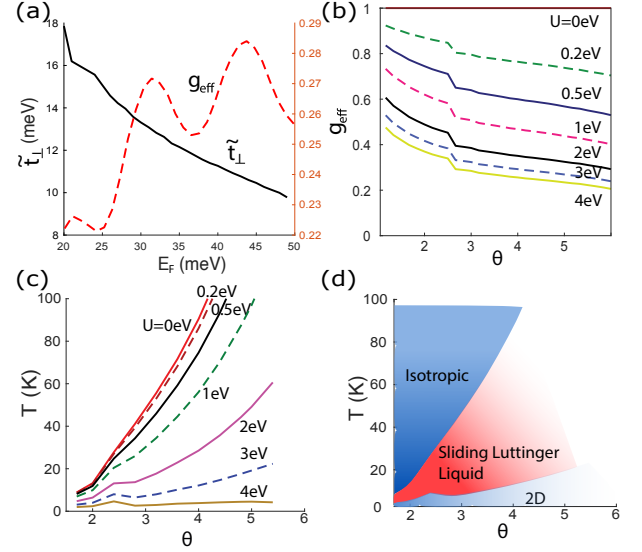


FIG. 3. (a) Plots of effective Luttinger parameter g_{eff} and interwire coupling \tilde{t}_\perp vs Fermi energy E_F at 5° and $U = 3\text{eV}$. The left y axis shows \tilde{t}_\perp and the right y axis shows g_{eff} . (b) Plot of g_{eff} versus twist angle θ for different U at Fermi energy $E_F = 30\text{meV}$. (c) The lower-bound SLL temperature T_* vs θ for different U at Fermi energy $E_F = 30\text{meV}$. (d) Phase diagram for a twisted system at different angles θ for $U = 3\text{eV}$ at Fermi energy $E_F = 30\text{meV}$. The upper and lower boundaries are crossover temperatures T_0 and T_* , respectively.

which is the key feature of SLL. The longitudinal conductivity σ_\parallel along the moiré wires [the y direction in Fig. 1(c)] is expected to be similar to that of the 1D Luttinger liquid, which increases as T decreases in the disorderless limit (diverging at $T = 0$, if temperature T could reach zero).

Physically, the SLL regime cannot persist to arbitrarily high temperature, since the Luttinger liquid theory is only valid at low energies. In the literature [4, 64], it is assumed that the upper bound temperature is $T_0 \sim \tilde{t}_\parallel / k_B$, which is a very high temperature. Here we argue that the upper bound temperature for the power law behavior of $\sigma_\perp(V, T)$ in Eq. (14) is much lower, due to the presence of marginal and irrelevant couplings (inelastic scattering with phonons, etc.). Note that $\sigma_\perp(V, T)$ in Eq. (13) considers only the relevant bare coupling \tilde{t}_\perp which has the unit of energy. In general, irrelevant couplings of dimension $-\Delta < 0$ would induce effective couplings scaling as $(k_B T)^\Delta$, which grows as T increases. Without a detailed knowledge of the irrelevant couplings, we expect their corrections to be no longer negligible when $k_B T > \tilde{t}_\perp$. This sets an upper bound crossover temperature for the SLL behavior as

$$T_0 \sim k_B^{-1} \tilde{t}_\perp, \quad (15)$$

which we adopt here. The SLL regime is thus within the temperature range $T_* < T < T_0$.

Fig. 3(c) shows the lower bound temperature T_* as a function of twist angle θ for $E_F = 30\text{meV}$ and interaction strength U ranging from 0 to 4eV, for which the Luttinger liquid parameter g_{eff} is shown in Fig. 2(b). Generically, we find that

T_* decreases as θ decreases, because of the decrease of \tilde{t}_\perp , although g_{eff} increases. As an example, Fig. 3(d) shows the phase diagram plotted for $E_F = 30\text{meV}$, $U = 3\text{eV}$ with respect to θ , where the lower and upper curves are the crossover temperatures T_* in Eq. (12) and T_0 and Eq. (15), respectively, in between which is the SLL regime. We note that T_* and T_0 are both order estimations. At temperatures $T > T_0$, one expects the anisotropy of the system to be suppressed by strong thermal fluctuations and irrelevant couplings, which we call the isotropic regime. For temperatures $T < T_*$ which we denote as the 2D regime, the perpendicular hopping \tilde{t}_\perp becomes important, and the system will behave intrinsically as a low temperature 2D system. As the temperature T decreases, depending on interactions, the system may remain a 2D Fermi liquid till $T = 0$, or undergo a symmetry breaking phase transition into charge density wave, etc., as studied in the literature [8–11].

Discussion. We have seen that for the effective coupled moiré wires, the Luttinger parameter g_{eff} (e.g., ~ 0.3 for $U = 3\text{eV}$) is much lower than the Luttinger parameter g (~ 0.6 for $U = 3\text{eV}$, see Appendix C) of the monolayer microscopic coupled wires. Generically, this is because of the lowering of Fermi velocity v_F and effectively longer range of interaction broadened by the widths of moiré wires. The lower bound temperature T_* of the SLL regime can be rather

sensitive to U . For our parameters, at $\theta = 5^\circ$, T_* drops from 50K to about 4K as U increases from 2 to 4eV. If U further increases, T_* would drop down to zero, leading to a zero-temperature SLL quantum phase. In the WTe₂ experiments [28, 29], $T_* \sim 2\text{K}$ at $\theta = 5^\circ$, and $T_* < 50\text{mK}$ at $\theta = 3^\circ$, which are similar to our results for $U \gtrsim 3\text{eV}$. This suggests that a strong microscopic interaction is needed to explain the experiments. Future studies with more accurate moiré models are needed for quantitative understandings. More generally, we expect our twisted coupled wire modeling to be applicable to twisted bilayers of 2D anisotropic systems, such as arrays of nanowires [5, 6], black phosphorus [65], etc., with different energy scales.

ACKNOWLEDGMENTS

Acknowledgments. We are thankful for helpful discussions with Tiancheng Song, Guo Yu, Pengjie Wang, Sanfeng Wu, and Jing Wang. This work is supported by the Alfred P. Sloan Foundation, by the National Science Foundation under award (DMR-2141966) and (DMR-2011750) through the Princeton University’s Materials Research Science and Engineering Center. Additional support was provided by the Gordon and Betty Moore Foundation through Grant No. GBMF8685 towards the Princeton theory program.

Appendix A: Transfer Matrix

In this section, we supplement details on how to obtain transfer matrix that helped us solving band structures for our bilayer system.

Since we have a network model of quantum wires, intersection points form a lattice \mathbb{Z}^2 . In real space, we can relate wave-

functions passing through a column of intersection points along y -direction using transfer matrix M :

$$\begin{pmatrix} \vdots \\ \psi_{+,n_y}^L(n_x a_x + 0^+) \\ \psi_{+,n_y}^R(n_x a_x + 0^+) \\ \psi_{-,n_y-n_x}^L(n_x a_x + 0^+) \\ \psi_{-,n_y-n_x}^R(n_x a_x + 0^+) \\ \psi_{+,n_y+1}^L(n_x a_x + 0^+) \\ \psi_{+,n_y+1}^R(n_x a_x + 0^+) \\ \psi_{-,n_y-n_x+1}^L(n_x a_x + 0^+) \\ \psi_{-,n_y-n_x+1}^R(n_x a_x + 0^+) \\ \vdots \end{pmatrix} = \begin{pmatrix} \ddots & & & & & & & & \\ 0 & 0 & 0 & 0 & 1 - \frac{i\lambda' m}{k} & -\frac{i\lambda' m}{k} & -\frac{i\lambda m}{k} & -\frac{i\lambda m}{k} \\ 0 & 0 & 0 & 0 & \frac{i\lambda' m}{k} & 1 + \frac{i\lambda' m}{k} & \frac{i\lambda m}{k} & \frac{i\lambda m}{k} \\ -\frac{i\lambda m}{k} & -\frac{i\lambda m}{k} & 1 - \frac{i\lambda' m}{k} & -\frac{i\lambda' m}{k} & 0 & 0 & 0 & 0 \\ \frac{i\lambda m}{k} & \frac{i\lambda m}{k} & \frac{i\lambda' m}{k} & 1 + \frac{i\lambda' m}{k} & 0 & 0 & 0 & 0 \\ 1 - \frac{i\lambda' m}{k} & -\frac{i\lambda' m}{k} & -\frac{i\lambda m}{k} & -\frac{i\lambda m}{k} & 0 & 0 & 0 & 0 \\ \frac{i\lambda' m}{k} & 1 + \frac{i\lambda' m}{k} & \frac{i\lambda m}{k} & \frac{i\lambda m}{k} & 0 & 0 & 0 & 0 \\ 0 & 0 & 0 & 0 & -\frac{i\lambda m}{k} & -\frac{i\lambda m}{k} & 1 - \frac{i\lambda' m}{k} & -\frac{i\lambda' m}{k} \\ 0 & 0 & 0 & 0 & \frac{i\lambda m}{k} & \frac{i\lambda m}{k} & \frac{i\lambda' m}{k} & 1 + \frac{i\lambda' m}{k} \\ & & & & & & \ddots & \end{pmatrix} \begin{pmatrix} \vdots \\ \psi_{+,n_y}^L(n_x a_x - 0^+) \\ \psi_{+,n_y}^R(n_x a_x - 0^+) \\ \psi_{-,n_y-n_x}^L(n_x a_x - 0^+) \\ \psi_{-,n_y-n_x}^R(n_x a_x - 0^+) \\ \psi_{+,n_y+1}^L(n_x a_x - 0^+) \\ \psi_{+,n_y+1}^R(n_x a_x - 0^+) \\ \psi_{-,n_y-n_x+1}^L(n_x a_x - 0^+) \\ \psi_{-,n_y-n_x+1}^R(n_x a_x - 0^+) \\ \vdots \end{pmatrix} \quad (\text{A1})$$

If we perform discrete Fourier transformation on the above transfer matrix M along y -direction, we obtain Eq. (4).

Appendix B: Inter and Intra-layer interactions

In this section, we present details on our calculations of $k = 0$ and $2q_y$ component of potential $V(\mathbf{r})$.

Moiré wavefunctions within a unit cell at momentum q_x, q_y is

$$\psi_{\alpha,q_y,q_x}(\mathbf{r}) = (\psi_{\alpha}^L e^{-ikx} + \psi_{\alpha}^R e^{ikx}) \quad (\text{B1})$$

where $\mathbf{r} = (x, -\alpha \frac{a_y}{a_x} x, \alpha \frac{a_z}{2})$ and $a_z = 0.77\text{nm}$ is the interlayer distance. We require wavefunction be normalized in a unit cell:

$$\sum_{\alpha=\pm} \int_{uc} d\mathbf{r} |\psi_{\alpha,q_y,q_x}(\mathbf{r})|^2 = 1 \quad (\text{B2})$$

where the integration is over along wires within a unit cell (abbreviated as “uc”). Unit cell “area” are total lengths within a unit cell which equals $2a_x$.

For a stripe S, an vertical array of unit cells that host a single moiré wire (1d), Fourier transformed interaction potential at momentum q

$$\tilde{V}(q) = a_y \sum_{\alpha,\alpha'=\pm} \int_{uc} d\mathbf{r} \int_S d\mathbf{r}' \psi_{\alpha,q_1+q}^{\dagger}(\mathbf{r}) \psi_{\alpha,q_1}(\mathbf{r}) \psi_{\alpha',q_2-q}^{\dagger}(\mathbf{r}') \psi_{\alpha',q_2}(\mathbf{r}') V(\mathbf{r} - \mathbf{r}') \quad (\text{B3})$$

where q_x is omitted for simplicity.

With

$$\psi_{\alpha,q_y}(\mathbf{r} + a_y \hat{y}) = e^{iq_y a_y} \psi_{\alpha,q_y}(\mathbf{r}), \quad (\text{B4})$$

and if there are further n th neighbour interactions in y direction with V_I^n is symmetric in y -direction then the two Fourier components of potential at $k = 0$ and $2q_F$ are

$$\begin{aligned}\tilde{V}(0) &= a_y \sum_{\alpha, \alpha' = \pm} \int_{uc} d\mathbf{r} \int_{uc} d\mathbf{r}' \psi_{\alpha, q_F}^\dagger(\mathbf{r}) \psi_{\alpha, q_F}(\mathbf{r}) \psi_{\alpha', -q_F}^\dagger(\mathbf{r}') \psi_{\alpha', -q_F}(\mathbf{r}') \left(\sum_{n=-\infty}^{\infty} V_I(\mathbf{r} - \mathbf{r}' + na_y \hat{y}) \right) \\ \tilde{V}(2q_F) &= a_y \sum_{\alpha, \alpha' = \pm} \int_{uc} d\mathbf{r} \int_{uc} d\mathbf{r}' \psi_{\alpha, q_F}^\dagger(\mathbf{r}) \psi_{\alpha, -q_F}(\mathbf{r}) \psi_{\alpha', -q_F}^\dagger(\mathbf{r}') \psi_{\alpha', q_F}(\mathbf{r}') \left(\sum_{n=-\infty}^{\infty} V_I(\mathbf{r} - \mathbf{r}' + na_y \hat{y}) \cos(2nq_F a_y) \right)\end{aligned}\quad (\text{B5})$$

where

$$V_I(\mathbf{r}) = U \exp \left(-\sqrt{\frac{x^2}{x_0^2} + \frac{y^2}{y_0^2} + \frac{z^2}{z_0^2}} \right) \quad (\text{B6})$$

as we defined in the main text, where $x_0 = 1\text{nm}$, $y_0 = 5\text{nm}$, $z_0 = 10\text{nm}$. For our numerical calculations, we take a cutoff of $|n| \leq 6$ nearest unit cells along y -direction.

Appendix C: Monolayer WTe_2 Luttinger parameter estimation

In this section, we give a brief estimation of Luttinger parameter for a single layer of WTe_2 following similar reasons we give in this paper.

In monolayer case, we have our interaction potential along the direction of the wire (x direction) in momentum space as

$$V_I(k) = \frac{2Ux_0}{1 + k^2x_0^2} \quad (\text{C1})$$

where $x_0 = 1\text{nm}$. Therefore, the effective Luttinger parameter is again given by

$$g_{\text{eff}} = \sqrt{\frac{2\pi v_F^{(0)} + V_I(2k_F)}{2\pi v_F^{(0)} + 2V_I(0) - V_I(2k_F)}}, \quad (\text{C2})$$

where $v_F^{(0)} = \frac{\hbar^2 k_F}{m}$ is the Fermi velocity of the microscopic wire, and $\hbar k_F = \sqrt{2mE_F}$. For different interaction strength U with $E_F = 30\text{meV}$, we have

	$U = 0.2\text{eV}$	0.5eV	1eV	2eV	3eV	4eV
g_{eff}	0.82	0.72	0.65	0.6	0.59	0.58

Appendix D: Interwire hopping parameter estimation from ab initio calculations

The first-principle calculations were performed on the Vienna ab initio simulation package[49, 50]. The generalized gradient approximation with the Perdew-Burke-Ernzerhof type exchange-correlation potential was adopted[51]. The convergence accuracy of self-consistent calculations is 10^{-6} eV per unit cell by using k grids with a $11 \times 11 \times 1$ mesh. We constructed the tight-binding Hamiltonian of the monolayer WTe_2 using the Wannier90 package[66] and generated the maximally localized Wannier functions for $5d$ orbitals on tungsten and $5p$ orbitals on tellurium.

Based on the tight-binding Hamiltonian from Wannier calculations, we estimate the interwire hopping parameter t_\perp within each layer. Under the Wannier function basis, i.e., $\{d_{z2}^\alpha, d_{xz}^\alpha, d_{yz}^\alpha, d_{x2-y2}^\alpha, d_{xy}^\alpha\}$ where α represents the two W atoms in one unit cell, the wave function of the top valence band at the Γ point $|\Psi\rangle_v$ is expressed as,

$$|\Psi\rangle_v = \sum_i c_i |\phi\rangle_i \quad (\text{D1})$$

where $i = 1, 2, \dots, 10$ is the index of Wannier function basis $|\phi\rangle_i$. Then the interwire hopping parameter t_\perp is estimated by the following equation,

$$t_\perp = \sum_{m \in C_1, n \in C_2} c_m^* c_n t_{mn} \quad (\text{D2})$$

where t_{mn} is the hopping strength between the Wannier orbital $|\psi_m\rangle$ in wire C_1 and the Wannier orbital $|\psi_n\rangle$ in wire C_2 . This yields $t_\perp \approx 20\text{meV}$.

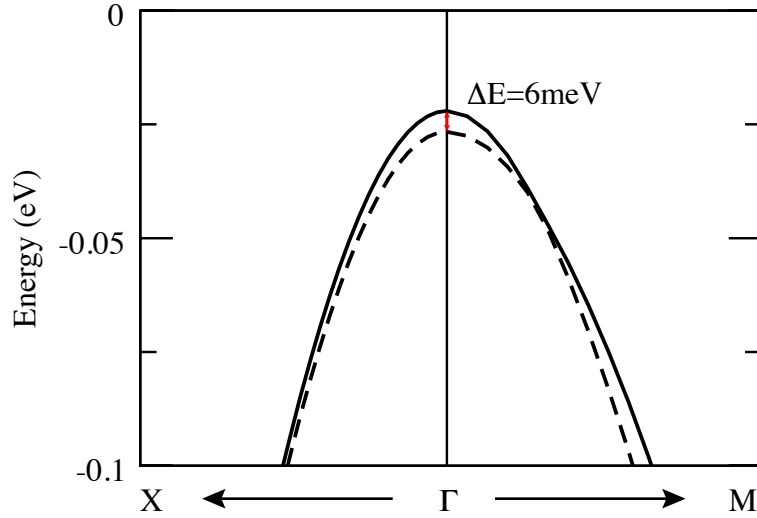


FIG. 4. Band structure calculation for a bilayer-structure WTe_2 nearby the Γ point. As indicated by the red arrow line, due to the interlayer coupling, there is a hybridization band gap $\Delta E = 6$ meV for the top valence bands around the Γ point.

Appendix E: Interlayer hopping of strength

Based on the first principle calculations, we also obtained the interlayer hopping of strength. As shown in Fig. 4, the hybridization band gap between the top and bottom WTe_2 layers is about $\Delta E = 6$ meV. In the effective moiré model we consider, the delta function interlayer hopping strength λ' is roughly the interlayer hopping energy times the spatial range of the interlayer hopping. For two wires in different layers, the two wires are close within the length scale of the x direction moiré lattice constant $a_x = \frac{l}{2\sin(\theta/2)}$, so we regard a_x as the spatial range of interlayer hopping. For angles $\theta \lesssim 5^\circ$ we consider, with $l = 0.627$ nm, we have $a_x \gtrsim 6$ nm, and thus we estimate the delta function interlayer hopping strength as $\lambda' \approx \Delta E a_x / 2 \approx 20$ meV \cdot nm.

For the intralayer delta function potential λ from the other layer, we adopt $\lambda \approx 10$ meV \cdot nm, which has the same order of magnitude magnitude following a similar argument as above.

We note that these parameters are by no means aimed to characterize WTe_2 accurately, since the coupled wire model we study is an oversimplified description to such moiré systems. The procedure is to ensure the parameters are within the reasonable ranges of physical materials.

-
- [1] S. i. Tomonaga, Remarks on bloch's method of sound waves applied to many-fermion problems, *Progress of Theoretical Physics* **5**, 544 (1950).
 - [2] F. D. M. Haldane, 'luttinger liquid theory' of one-dimensional quantum fluids. i. properties of the luttinger model and their extension to the general 1d interacting spinless fermi gas, *Journal of Physics C: Solid State Physics* **14**, 2585 (1981).
 - [3] J. M. Luttinger, An exactly soluble model of a many-fermion system, *Journal of Mathematical Physics* **4**, 1154 (1963).
 - [4] T. Giamarchi, *Quantum Physics in One Dimension* (Oxford University Press, 2003).
 - [5] S. Wang, S. Zhao, Z. Shi, F. Wu, Z. Zhao, L. Jiang, K. Watanabe, T. Taniguchi, A. Zettl, C. Zhou, and F. Wang, Nonlinear luttinger liquid plasmons in semiconducting single-walled carbon nanotubes, *Nature Materials* **19**, 986–991 (2020).
 - [6] Y. Jompol, C. J. B. Ford, J. P. Griffiths, I. Farrer, G. A. C. Jones, D. Anderson, D. A. Ritchie, T. W. Silk, and A. J. Schofield, Probing spin-charge separation in a tomonaga-luttinger liquid, *Science* **325**, 597–601 (2009).
 - [7] X. G. Wen, Metallic non-fermi-liquid fixed point in two and higher dimensions, *Phys. Rev. B* **42**, 6623 (1990).
 - [8] V. J. Emery, E. Fradkin, S. A. Kivelson, and T. C. Lubensky, Quantum theory of the smectic metal state in stripe phases, *Phys. Rev. Lett.* **85**, 2160 (2000).
 - [9] S. L. Sondhi and K. Yang, Sliding phases via magnetic fields, *Phys. Rev. B* **63**, 054430 (2001).
 - [10] A. Vishwanath and D. Carpentier, Two-dimensional anisotropic non-fermi-liquid phase of coupled luttinger liquids, *Phys. Rev. Lett.* **86**, 676 (2001).
 - [11] R. Mukhopadhyay, C. L. Kane, and T. C. Lubensky, Sliding luttinger liquid phases, *Phys. Rev. B* **64**, 045120 (2001).
 - [12] J. C. Y. Teo and C. L. Kane, From luttinger liquid to non-abelian quantum hall states, *Phys. Rev. B* **89**, 085101 (2014).
 - [13] C. L. Kane, A. Stern, and B. I. Halperin, Pairing in luttinger liquids and quantum hall states, *Phys. Rev. X* **7**, 031009 (2017).
 - [14] Y. Fuji and P. Lecheminant, Non-abelian $su(n-1)$ -singlet fractional quantum hall states from coupled wires, *Phys. Rev. B* **95**, 125130 (2017).
 - [15] C. L. Kane and A. Stern, Coupled wire model of Z_4 orbifold quantum hall states, *Phys. Rev. B* **98**, 085302 (2018).

- [16] Y. Imamura, K. Totsuka, and T. H. Hansson, From coupled-wire construction of quantum hall states to wave functions and hydrodynamics, *Phys. Rev. B* **100**, 125148 (2019).
- [17] P. M. Tam, Y. Hu, and C. L. Kane, Coupled wire model of $Z_2 \times Z_2$ orbifold quantum hall states, *Phys. Rev. B* **101**, 125104 (2020).
- [18] P. M. Tam and C. L. Kane, Nondiagonal anisotropic quantum hall states, *Phys. Rev. B* **103**, 035142 (2021).
- [19] T. Neupert, C. Chamon, C. Mudry, and R. Thomale, Wire deconstructionism of two-dimensional topological phases, *Phys. Rev. B* **90**, 205101 (2014).
- [20] T. Iadecola, T. Neupert, C. Chamon, and C. Mudry, Wire constructions of abelian topological phases in three or more dimensions, *Phys. Rev. B* **93**, 195136 (2016).
- [21] Y. Fuji and A. Furusaki, From coupled wires to coupled layers: Model with three-dimensional fractional excitations, *Phys. Rev. B* **99**, 241107 (2019).
- [22] T. Meng, T. Neupert, M. Greiter, and R. Thomale, Coupled-wire construction of chiral spin liquids, *Phys. Rev. B* **91**, 241106 (2015).
- [23] A. A. Patel and D. Chowdhury, Two-dimensional spin liquids with F_2 topological order in an array of quantum wires, *Phys. Rev. B* **94**, 195130 (2016).
- [24] J. C. Y. Teo and Y. Hu, Dihedral twist liquid models from emergent majorana fermions, *Quantum* **7**, 967 (2023).
- [25] A. Georges, T. Giamarchi, and N. Sandler, Interchain conductivity of coupled luttinger liquids and organic conductors, *Phys. Rev. B* **61**, 16393 (2000).
- [26] X. Du, L. Kang, Y. Y. Lv, J. S. Zhou, X. Gu, R. Z. Xu, Q. Q. Zhang, Z. X. Yin, W. X. Zhao, Y. D. Li, S. M. He, D. Pei, Y. B. Chen, M. X. Wang, Z. K. Liu, Y. L. Chen, and L. X. Yang, Crossed luttinger liquid hidden in a quasi-two-dimensional material, *Nature Physics* **19**, 40 (2022).
- [27] L. Niu, S. Jin, X. Chen, X. Li, and X. Zhou, Observation of a dynamical sliding phase superfluid with p -band bosons, *Phys. Rev. Lett.* **121**, 265301 (2018).
- [28] P. Wang, G. Yu, Y. H. Kwan, Y. Jia, S. Lei, S. Klemen, F. A. Cevallos, R. Singha, T. Devakul, K. Watanabe, T. Taniguchi, S. L. Sondhi, R. J. Cava, L. M. Schoop, S. A. Parameswaran, and S. Wu, One-dimensional luttinger liquids in a two-dimensional moiré lattice, *Nature* **605**, 57 (2022).
- [29] G. Yu, P. Wang, A. J. Uzan-Narovlansky, Y. Jia, M. Onyszcak, R. Singha, X. Gui, T. Song, Y. Tang, K. Watanabe, T. Taniguchi, R. J. Cava, L. M. Schoop, and S. Wu, Evidence for two dimensional anisotropic luttinger liquids at millikelvin temperatures, *Nature Communications* **14**, 10.1038/s41467-023-42821-2 (2023).
- [30] L. Balents, C. R. Dean, D. K. Efetov, and A. F. Young, Superconductivity and strong correlations in moiré flat bands, *Nature Physics* **16**, 725 (2020).
- [31] F. Haddadi, Q. Wu, A. J. Kruchkov, and O. V. Yazyev, Moiré flat bands in twisted double bilayer graphene, *Nano Letters* **20**, 2410 (2020).
- [32] H. Li, S. Li, M. H. Naik, J. Xie, X. Li, J. Wang, E. Regan, D. Wang, W. Zhao, S. Zhao, S. Kahn, K. Yumigeta, M. Blei, T. Taniguchi, K. Watanabe, S. Tongay, A. Zettl, S. G. Louie, F. Wang, and M. F. Crommie, Imaging moiré flat bands in three-dimensional reconstructed WSe₂/WS₂ superlattices, *Nature Materials* **20**, 945 (2021).
- [33] Y. Tang, L. Li, T. Li, Y. Xu, S. Liu, K. Barmak, K. Watanabe, T. Taniguchi, A. H. MacDonald, J. Shan, and K. F. Mak, Simulation of hubbard model physics in WSe₂/WS₂ moiré superlattices, *Nature* **579**, 353 (2020).
- [34] F. Wu, T. Lovorn, E. Tutuc, and A. H. MacDonald, Hubbard model physics in transition metal dichalcogenide moiré bands, *Phys. Rev. Lett.* **121**, 026402 (2018).
- [35] Y. Shimazaki, I. Schwartz, K. Watanabe, T. Taniguchi, M. Kroner, and A. Imamoğlu, Strongly correlated electrons and hybrid excitons in a moiré heterostructure, *Nature* **580**, 472 (2020).
- [36] E. C. Regan, D. Wang, C. Jin, M. I. B. Utama, B. Gao, X. Wei, S. Zhao, W. Zhao, Z. Zhang, K. Yumigeta, M. Blei, J. D. Carlström, K. Watanabe, T. Taniguchi, S. Tongay, M. Crommie, A. Zettl, and F. Wang, Mott and generalized wigner crystal states in WSe₂/WS₂ moiré superlattices, *Nature* **579**, 359 (2020).
- [37] M. Yankowitz, S. Chen, H. Polshyn, Y. Zhang, K. Watanabe, T. Taniguchi, D. Graf, A. F. Young, and C. R. Dean, Tuning superconductivity in twisted bilayer graphene, *Science* **363**, 1059 (2019).
- [38] X. Liu, Z. Hao, E. Khalaf, J. Y. Lee, Y. Ronen, H. Yoo, D. H. Najafabadi, K. Watanabe, T. Taniguchi, A. Vishwanath, and P. Kim, Tunable spin-polarized correlated states in twisted double bilayer graphene, *Nature* **583**, 221 (2020).
- [39] K. Kim, A. DaSilva, S. Huang, B. Fallahazad, S. Larentis, T. Taniguchi, K. Watanabe, B. J. LeRoy, A. H. MacDonald, and E. Tutuc, Tunable moiré bands and strong correlations in small-twist-angle bilayer graphene, *Proceedings of the National Academy of Sciences* **114**, 3364 (2017).
- [40] X. Lu, P. Stepanov, W. Yang, M. Xie, M. A. Aamir, I. Das, C. Urgell, K. Watanabe, T. Taniguchi, G. Zhang, A. Bachtold, A. H. MacDonald, and D. K. Efetov, Superconductors, orbital magnets and correlated states in magic-angle bilayer graphene, *Nature* **574**, 653 (2019).
- [41] Y. Cao, V. Fatemi, A. Demir, S. Fang, S. L. Tomarken, J. Y. Luo, J. D. Sanchez-Yamagishi, K. Watanabe, T. Taniguchi, E. Kaxiras, R. C. Ashoori, and P. Jarillo-Herrero, Correlated insulator behaviour at half-filling in magic-angle graphene superlattices, *Nature* **556**, 80 (2018).
- [42] Y. Cao, V. Fatemi, S. Fang, K. Watanabe, T. Taniguchi, E. Kaxiras, and P. Jarillo-Herrero, Unconventional superconductivity in magic-angle graphene superlattices, *Nature* **556**, 43 (2018).
- [43] G. W. Burg, J. Zhu, T. Taniguchi, K. Watanabe, A. H. MacDonald, and E. Tutuc, Correlated insulating states in twisted double bilayer graphene, *Phys. Rev. Lett.* **123**, 197702 (2019).
- [44] Y. Cao, D. Rodan-Legrain, O. Rubies-Bigorda, J. M. Park, K. Watanabe, T. Taniguchi, and P. Jarillo-Herrero, Tunable correlated states and spin-polarized phases in twisted bilayer-bilayer graphene, *Nature* **583**, 215 (2020).
- [45] G. Chen, L. Jiang, S. Wu, B. Lyu, H. Li, B. L. Chittari, K. Watanabe, T. Taniguchi, Z. Shi, J. Jung, Y. Zhang, and F. Wang, Evidence of a gate-tunable mott insulator in a trilayer graphene moiré superlattice, *Nature Physics* **15**, 237 (2019).
- [46] C.-H. Hsu, D. Loss, and J. Klinovaja, General scattering and electronic states in a quantum-wire network of moiré systems, *Phys. Rev. B* **108**, L121409 (2023).
- [47] M. Angeli and A. H. MacDonald, Γ valley transition metal dichalcogenide moiré bands, *Proceedings of the National Academy of Sciences* **118**, 10.1073/pnas.2021826118 (2021).
- [48] S. Fang, R. Kuate Defo, S. N. Shirodkar, S. Lieu, G. A. Tritsaris, and E. Kaxiras, Ab initio tight-binding hamiltonian for transition metal dichalcogenides, *Phys. Rev. B* **92**, 205108 (2015).
- [49] G. Kresse and J. Furthmüller, Efficiency of ab-initio total energy calculations for metals and semiconductors using a plane-wave basis set, *Computational Materials Science* **6**, 15 (1996).
- [50] G. Kresse and J. Hafner, *Ab initio* molecular dynamics for open-shell transition metals, *Phys. Rev. B* **48**, 13115 (1993).
- [51] J. P. Perdew, K. Burke, and M. Ernzerhof, Generalized gradient approximation made simple, *Phys. Rev. Lett.* **77**, 3865 (1996).

- [52] B. Sun, W. Zhao, T. Palomaki, Z. Fei, E. Runburg, P. Malinowski, X. Huang, J. Cenker, Y.-T. Cui, J.-H. Chu, X. Xu, S. S. Ataei, D. Varsano, M. Palummo, E. Molinari, M. Rontani, and D. H. Cobden, Evidence for equilibrium exciton condensation in monolayer WTe₂, *Nature Physics* **18**, 94 (2021).
- [53] Y. Jia, P. Wang, C.-L. Chiu, Z. Song, G. Yu, B. Jäck, S. Lei, S. Klemen, F. A. Cevallos, M. Onyszczyk, N. Fishchenko, X. Liu, G. Farahi, F. Xie, Y. Xu, K. Watanabe, T. Taniguchi, B. A. Bernevig, R. J. Cava, L. M. Schoop, A. Yazdani, and S. Wu, Evidence for a monolayer excitonic insulator, *Nature Physics* **18**, 87 (2021).
- [54] R. Jing, Y. Shao, Z. Fei, C. F. B. Lo, R. A. Vitalone, F. L. Ruta, J. Staunton, W. J.-C. Zheng, A. S. Mcleod, Z. Sun, B. yuan Jiang, X. Chen, M. M. Fogler, A. J. Millis, M. Liu, D. H. Cobden, X. Xu, and D. N. Basov, Terahertz response of monolayer and few-layer wte2 at the nanoscale, *Nature Communications* **12**, 10.1038/s41467-021-23933-z (2021).
- [55] J. Kwak, Y. Jo, S. Song, J. H. Kim, S.-Y. Kim, J.-U. Lee, S. Lee, J. Park, K. Kim, G.-D. Lee, J.-W. Yoo, S. Y. Kim, Y.-M. Kong, G.-H. Lee, W.-G. Lee, J. Park, X. Xu, H. Cheong, E. Yoon, Z. Lee, and S.-Y. Kwon, Single-crystalline nanobelts composed of transition metal ditellurides, *Advanced Materials* **30**, 1707260 (2018).
- [56] G.-B. Liu, D. Xiao, Y. Yao, X. Xu, and W. Yao, Electronic structures and theoretical modelling of two-dimensional group-VIB transition metal dichalcogenides, *Chemical Society Reviews* **44**, 2643 (2015).
- [57] V. Crépel and L. Fu, Spin-triplet superconductivity from excitonic effect in doped insulators, *Proceedings of the National Academy of Sciences* **119**, 10.1073/pnas.2117735119 (2022).
- [58] S. Tang, C. Zhang, D. Wong, Z. Pedramrazi, H.-Z. Tsai, C. Jia, B. Moritz, M. Claassen, H. Ryu, S. Kahn, J. Jiang, H. Yan, M. Hashimoto, D. Lu, R. G. Moore, C.-C. Hwang, C. Hwang, Z. Hussain, Y. Chen, M. M. Ugeda, Z. Liu, X. Xie, T. P. Devereaux, M. F. Crommie, S.-K. Mo, and Z.-X. Shen, Quantum spin hall state in monolayer 1t'-wte2, *Nature Physics* **13**, 683 (2017).
- [59] Y. H. Kwan, T. Devakul, S. L. Sondhi, and S. A. Parameswaran, Theory of competing excitonic orders in insulating wte₂ monolayers, *Phys. Rev. B* **104**, 125133 (2021).
- [60] A. N. Domozhirova, A. A. Makhnev, E. I. Shreder, S. V. Naumov, A. V. Lukoyanov, V. V. Chistyakov, J. C. A. Huang, A. A. Semiannikova, P. S. Korenistov, and V. V. Marchenkov, Electronic properties of wte2 and mote2 single crystals, *Journal of Physics: Conference Series* **1389**, 012149 (2019).
- [61] M. P. A. Fisher and L. I. Glazman, Transport in a one-dimensional luttinger liquid, in *Mesoscopic Electron Transport* (Springer Netherlands, 1997) pp. 331–373.
- [62] C. Bourbonnais, F. Creuzet, D. Jérôme, K. Bechgaard, and A. Moradpour, Cooperative phenomena in (TMTSF)₂clo₄ : an NMR evidence, *Journal de Physique Lettres* **45**, 755 (1984).
- [63] E. Fradkin, *Field Theories of Condensed Matter Physics* (Cambridge University Press, 2013).
- [64] S. Biermann, A. Georges, T. Giamarchi, and A. Lichtenstein, Quasi one-dimensional organic conductors: Dimensional crossover and some puzzles, in *Strongly Correlated Fermions and Bosons in Low-Dimensional Disordered Systems* (Springer Netherlands, 2002) pp. 81–102.
- [65] H. Wang, Z. Liu, Y. Jiang, and J. Wang, Giant anisotropic band flattening in twisted Γ -valley semiconductor bilayers, *Phys. Rev. B* **108**, L201120 (2023).
- [66] G. Pizzi, V. Vitale, R. Arita, S. Blügel, F. Freimuth, G. Géranton, M. Gibertini, D. Gresch, C. Johnson, T. Koretsune, J. Ibañez-Azpiroz, H. Lee, J.-M. Lihm, D. Marchand, A. Marrazzo, Y. Mokrousov, J. I. Mustafa, Y. Nohara, Y. Nomura, L. Paulatto, S. Poncé, T. Ponweiser, J. Qiao, F. Thöle, S. S. Tsirkin, M. Wierzbowska, N. Marzari, D. Vanderbilt, I. Souza, A. A. Mostofi, and J. R. Yates, Wannier90 as a community code: new features and applications, *Journal of Physics: Condensed Matter* **32**, 165902 (2020).